NUCL SCI TECH (2019) 30:65
https://doi.org/10.1007/s41365-019-0586-2

Creep damage characterization of UNS N10003 alloy based on a numerical simulation using the Norton creep law and Kachanov–Rabotnov creep damage model

Xiao-Yan Wang[1,2] · Xiao Wang[1] · Xiao-Chun Zhang[1] · Shi-Feng Zhu[1]

Received: 18 July 2018 / Revised: 20 September 2018 / Accepted: 1 October 2018 / Published online: 21 March 2019

Abstract The calculation of inelastic creep damage is important for the structural integrity evaluation of the elevated temperature structure in a thorium molten salt reactor (TMSR). However, a creep damage theory model and numerical simulation method have not been proposed for the key materials (UNS N10003 alloy) in the TMSR. In this study, creep damage characterization of UNS N10003 alloy is investigated using the Norton creep law and Kachanov–Rabotnov (K–R) creep damage model. First, the creep experimental data of the UNS N10003 alloy at 650 °C were adopted to fit the material constants of the two models. Then, the creep damage behavior of the UNS N10003 alloy was analyzed and discussed under uniaxial and multi-axial stress states. The results indicated that the K–R creep damage model is more suitable for the UNS N10003 alloy than the Norton model. Finally, the numerical simulation method was developed by a user-defined UMAT subroutine and subsequently verified through a finite element analysis (FEA). The FEA results were in agreement with the theoretical solutions. This study provides an effective method for the inelastic creep damage analysis of the elevated temperature structure in the TMSR.

The work was supported by the Strategic Priority Research Program of the Chinese Academy of Sciences (No. XDA02010000).

✉ Xiao Wang
wangxiao@sinap.ac.cn

✉ Xiao-Chun Zhang
zhangxiaochun@sinap.ac.cn

[1] Shanghai Institute of Applied Physics, Chinese Academy of Sciences, Shanghai 201800, China

[2] University of Chinese Academy of Sciences, Beijing 100049, China

Keywords Thorium molten salt reactor · UNS N10003 alloy · Creep damage · Inelastic analysis · Elevated temperature structure

1 Introduction

One of the six fourth-generation reactor candidates, the thorium molten salt reactor (TMSR), is safe and economical and contains low levels of nuclear waste and an adequate anti-proliferation performance [1–3]. Nickel-based UNS N10003 alloy has been applied in the TMSR with a strong corrosion resistance and high creep durability in the high-temperature molten salt environment. Because the metallic components are designed to operate during long-term service at 650 °C, an important property of the structures is the time-dependent creep behavior. Therefore, a precise calculation of the creep damage is important for the structural integrity assessment at an elevated temperature in the TMSR.

An elastic analysis method in the ASME-III-NH code [4] is widely used in high-temperature nuclear reactors to calculate and evaluate the creep damage [5–8]. However, if the creep effects are presumed significant or if the elastic analysis rules have not been satisfied, an inelastic analysis is required to provide a quantitative assessment of the creep deformation and creep damage. Yousefpour et al. [9] assessed the creep fracture life for the level-2 probabilistic safety assessment (PSA) of a 2-loop pressurized water reactor (PWR) with the Larson–Miller model. Yu et al. [10] carried out an inelastic creep analysis of a sodium-cooled fast reactor (SFR) based on the Norton creep law [11]. Mao et al. [12] studied and analyzed the high-temperature creep behavior of package shell candidate

materials (Hastelloy C276 alloy) of a supercritical water reactor (SCWR) using the Kachanov–Rabotnov (K–R) creep damage model [13–15]. Du et al. [16] simulated the creep damage of 2.25Cr–1Mo steel pressure vessels with defects based on the K–R model. Niu et al. [17, 18] calculated the creep damage of the high-temperature main steam pipeline (10CrMo910 steel) based on the K–R model. However, there have been minimal studies employing the inelastic creep damage constitutive model and numerical simulation method for the UNS N10003 alloy in the TMSR.

The remainder of the paper is organized as follows: In Sect. 2, the creep damage characterization of the UNS N10003 alloy is investigated based on continuum damage mechanics [19]. The Norton creep model and K–R creep damage model are obtained and analyzed. In Sect. 3, the numerical simulation method is developed and verified through a finite element analysis (FEA). The conclusion is provided in Sect. 4.

2 Theoretical models

2.1 Multi-axial creep damage model

The creep damage model based on the Norton creep law can be expressed as follows [11]:

$$\dot{\varepsilon}^* = C_1 \sigma_{\mathrm{eq}}^{C_2}, \tag{1}$$

$$\omega = 1 - (\dot{\varepsilon}^*/\dot{\varepsilon})^{1/C_2}, \tag{2}$$

where $\dot{\varepsilon}^*$ denotes the minimum creep strain rate; $\dot{\varepsilon}$ denotes the creep strain rate in tertiary creep stages; σ_{eq} denotes equivalent stress; ω denotes creep damage; C_1 and C_2 are material constants. The damage value from Eq. (2) is determined by the tested creep strain rate, which is generally used as the experimental values to assess the creep damage of elevated temperature structures.

The general form of the K–R creep damage model [20, 21] under the multi-axis stress state is as follows:

$$\dot{\varepsilon}_{ij}^c = \frac{3}{2}\frac{B\sigma_{\mathrm{eq}}^{n-1}S_{ij}}{(1-\omega)^n}, \tag{3}$$

$$\dot{\omega} = \frac{A\sigma_{\mathrm{r}}^p}{(1-\omega)^q}, \tag{4}$$

where $\dot{\varepsilon}_{ij}^c$ denotes multi-axial creep strain rate; $\dot{\omega}$ denotes creep damage rate; S_{ij} denotes deviation stress tensor; σ_{eq} denotes equivalent stress; $\sigma_{\mathrm{r}} = \left(\alpha\sigma_{\max} + (1-\alpha)\sigma_{\mathrm{eq}}\right)$ denotes reference stress; $\sigma_{\max}$ denotes maximum stress; A, B, n, p, q are material constants, which can be fitted by uniaxial creep test. α is a material constant related to the multi-axis stress state, which ranges from zero to unity.

2.2 Material constant fitting

The chemical composition and mechanical properties at room temperature of the UNS N10003 alloy are listed in Tables 1 and 2, respectively [22].

According to the standard test methods in ASTM E139-11, uniaxial creep tests were conducted at the Shanghai Institute of Applied Physics. Smooth round bar specimens with a diameter of 8 mm were measured using the Zwick/Roell KAPPA50 LA creep testing machine and the HBM high-temperature extensometer at 650 °C. The applied constant stresses (σ) were 250 MPa, 275 MPa, 320 MPa, and 380 MPa. The experimental creep strain (ε_{c}) versus time (t) with different stress levels at 650 °C was plotted, as shown in Fig. 1.

The primary creep, secondary creep, and tertiary creep stages are unclear for the UNS N10003 alloy under the higher stress level. The primary and secondary creep strains are low, and the tertiary creep governs the total creep deformation. For the higher stress range (σ = 380 MPa), the tertiary creep is present for a short time and thus reveals an approximate linearity as a function of time t. For the lower stress range (σ = 250 $\sim$ 320 MPa), the tertiary creep stages show an obvious acceleration process.

The values of the creep fracture time (t_{r}), creep fracture strain (ε_{r}), and minimum creep strain rate ($\dot{\varepsilon}^*$) at different stresses are obtained from the creep test of the UNS N10003 alloy at 650 °C, which are listed in Table 3.

According to the creep test data of the UNS N10003 alloy at 650 °C, the Norton creep model and K–R creep damage model are adopted for fitting the material constants. The units of time and stress in this study are h and MPa, respectively.

2.2.1 Norton model

The equation of $\ln(\dot{\varepsilon}^*) = \ln(C_1) + C_2\ln(\sigma_{\mathrm{eq}})$ can be obtained by taking the natural logarithm of both sides of Eq. (1). The equivalent stress σ_{eq} in the Norton model is equal to the applied stress σ. The linear fitting curve is shown in Fig. 2, and the coefficient of determination R-squared between the fitted values and experimental data is greater than 0.99. The two obtained material constants are $C_1 = 1.98 \times 10^{-18}$ and $C_2 = 5.79$, respectively.

2.2.2 K–R model

In order to fit the material constants of the K–R model, the expressions of the creep strain and creep damage are derived in this section. Integrating Eq. (4) with the initial condition of $\omega|_{t=t_{\mathrm{r}}} = 1$, the equation of the creep fracture

Table 1 Chemical composition of the UNS N10003 alloy (wt%)

Cr	Fe, max	C	Si, max	Co, max	Mn, max	W, max	V, max
6.0–8.0	5.0	0.04–0.08	1.00	0.20	1.00	0.50	0.50

Mo	P, max	S, max	Al + Ti, max	Cu, max	B, max	Ni
15.0–18.0	0.015	0.020	0.50	0.35	0.010	Remainder

Table 2 Mechanical properties at room temperature of the UNS N10003 alloy

Yield strength (0.2% offset) (MPa)	Tensile strength (MPa)	Elongation (%)
280	690	35

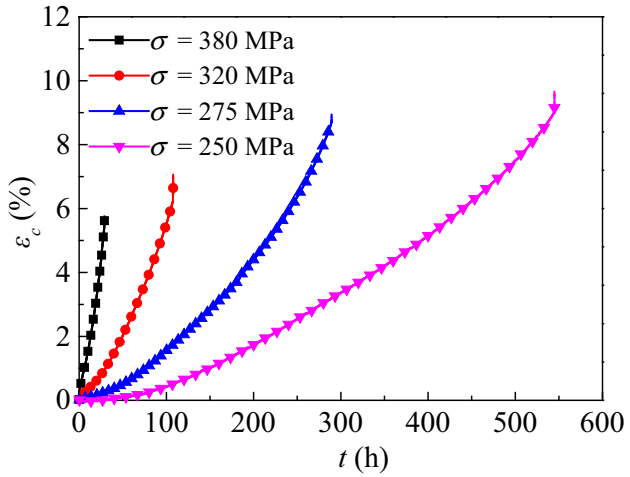

Fig. 1 (Color online) Experimental creep strain–time curves with different stresses for the UNS N10003 alloy at 650 °C

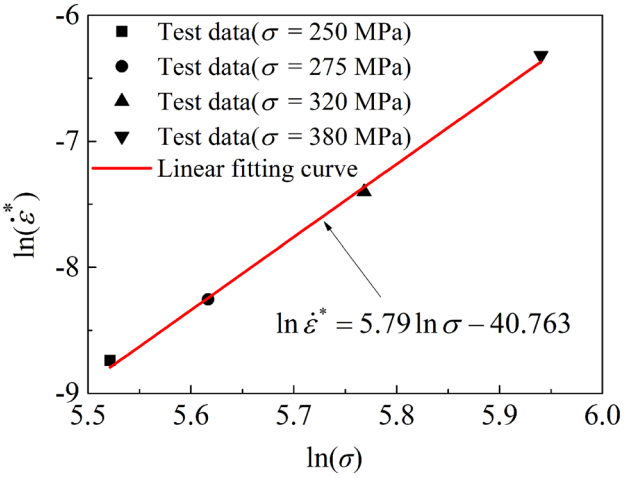

Fig. 2 Fitting curve of the Norton model

Table 3 Creep experimental data of the UNS N10003 alloy at 650 °C

σ (MPa)	t_r (h)	ε_r	$\dot{\varepsilon}^*$
250	545.1	0.0965	0.00016
275	289.5	0.0894	0.00026
320	107.9	0.0706	0.00061
380	29.10	0.0576	0.00180

time (t_r) and creep damage (ω) under the multi-axial stress state can be obtained.

$$t_r = 1/\left[A\sigma_r^p(q+1)\right] \tag{5}$$

$$\omega = 1-(1-t/t_r)^{1/(q+1)} \tag{6}$$

Substituting Eqs. (5) and (6) into Eq. (3), the equation of the multi-axial creep strain (ε_{ij}^c) can be derived by integrating the variable t.

$$\varepsilon_{ij}^c = \frac{f(\sigma_{ij})t_r}{K}\left\{1-(1-\omega)^{(q+1-n)}\right\} \tag{7}$$

Then, the creep fracture strain $\varepsilon_r = \varepsilon_{ij}^c|_{t=t_r}$ can be deduced:

$$\varepsilon_r = f(\sigma_{ij})t_r/K, \tag{8}$$

where $K = (q+1-n)/(q+1)$; $f(\sigma_{ij}) = 1.5B\sigma_{eq}^{n-1}S_{ij}$.

Under the uniaxial stress state, Eqs. (5) and (8) are simplified with $\sigma_{max} = \sigma_{eq} = \sigma_r = \sigma$, $f(\sigma_{ij}) = B\sigma^n$, and $\varepsilon_{ij}^c = \varepsilon_c$. Using the natural logarithm for Eqs. (5) and (8) after transformation, two linear equations $\ln(1/t_r) = \ln[A(q+1)] + p\ln(\sigma)$ and $\ln(\varepsilon_r/t_r) = \ln[B/K] + n\ln(\sigma)$ are obtained and then fitted by the uniaxial creep test data. Hence, p = 6.97, n =5.69, $\ln(A(q+1)) = -44.815$, and $\ln(B/K) = -40.083$ are obtained. Furthermore, the equation of $\varepsilon_c/\varepsilon_r = 1-(1-t/t_r)^K$ is deduced by dividing Eqs. (7) and (8). Nonlinear curve fitting is performed and shown in Fig. 3. The coefficient of determination R-squared is greater than 0.98. Thus, K = 0.57 and q = 12.23 are obtained. Substituting q and K into $\ln(A(q+1))$ and $\ln(B/K)$, the constants A and B are also obtained.

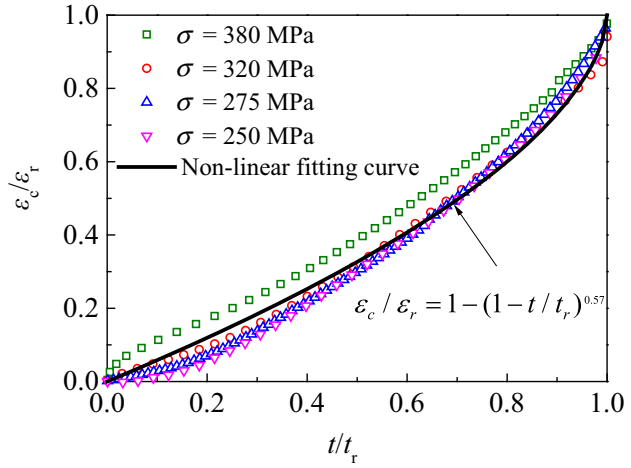

Fig. 3 Nonlinear fitting curve for the K–R model

The fitted material constants p, q, n, A, and B of the K–R creep damage model are listed in Table 4. In this study, the material constant α, which is unknown, is assumed to be 0.15 according to a nickel-base alloy (Waspaloy) in a previous study [23].

2.3 Analysis and discussion

According to Eqs. (1)–(4), the creep damage behavior is closely related to the stress state. Therefore, the above theoretical models are analyzed and discussed in detail based on the uniaxial and multi-axial stress states.

2.3.1 Uniaxial stress state

1. Creep strain analysis

The Norton and K–R models can describe the creep behavior of the UNS N10003 alloy under the uniaxial stress state. By integrating Eq. (1), the uniaxial Norton creep strain equation is obtained.

$$\varepsilon_c = 1.98 \times 10^{-18} \cdot \sigma^{5.79} \cdot t \tag{9}$$

By substituting the material constants (in Table 4) into Eqs. (5)–(7), the uniaxial K–R creep strain equation can also be derived as follows:

$$\varepsilon_c = 113.74/\sigma^{1.28} \cdot \left(1-\left(1-3.44 \times 10^{-20} \cdot \sigma^{6.97} \cdot t\right)^{0.57}\right) \tag{10}$$

Table 4 Material constants of the K–R creep damage model

A	B	p	q	n	α
2.6×10^{-21}	2.23×10^{-18}	6.97	12.23	5.69	0.15

The prediction curves of the creep strain obtained by these two equations (Eqs. (9) and (10)) are compared with the creep test data, as shown in Fig. 4a, b, respectively. The prediction curves from the Norton model are a linear function of time, and the curves from the K–R model are a power function of time under the constant stress state.

In order to analyze and evaluate the accuracy of the two theoretical models quantitatively, the residual sum of squares (RSS) and the coefficient of determination (R-square) of the creep strain between the theoretical prediction values and test data for the Norton and K–R models were calculated, as listed in Table 5. The RSS values of the K–R model were closer to zero, and the R-square values were closer to 1 than those of the Norton model, except for the higher stress level (σ = 380 MPa). These results indicated that the K–R model is more consistent with the test data and hence more suitable for describing the creep behavior of the UNS N10003 alloy than that of the Norton model.

Furthermore, the theoretical predicted values of the creep fracture time (t_r) and creep fracture strain (ε_r) of the K–R model are calculated and listed in Table 6. The maximum errors between the theoretical values and the test data are 7.27% for t_r and 4.20% for ε_r, which are within the allowable range. Consequently, the K–R model is more suitable than the Norton model for describing the creep characterization of the UNS N100003 alloy.

2. Creep damage analysis

The K–R theoretical creep damage equation can be obtained by substituting the material constants in Table 4 into Eq. (6) under the uniaxial stress state.

$$\omega = 1-(1-t/t_r)^{0.0756} \tag{11}$$

As mentioned, the Norton creep damage value in Eq. (2) can be considered as the tested damage value [12]. Thus, the K–R creep damage curve (theory results) with t/t_r is compared with the Norton creep damage values (test values), as shown in Fig. 5. The theoretical results are slightly higher than the test values at the same t/t_r. In engineering applications, the conservative theoretical results will be obtained by the K–R model. Therefore, the true damage of the structure will not reach the predicted values during the operation period. Thus, the K–R theory model is reliable for the structural safety design. According to Eqs. (5) and (6), the creep damage ω correlates with the stress σ, time t, and the material constant q under the uniaxial stress state. For the same t/t_r, the ω value is related to the material constant q, which is obtained by fitting the tested creep strain. In addition, Fig. 5 shows that creep damage occurs when $t > 0.9t_r$. When $t < 0.9t_r$, $\omega < 0.2$, which is less than the critical creep damage value of $\omega_{cr} = 1.0$. When

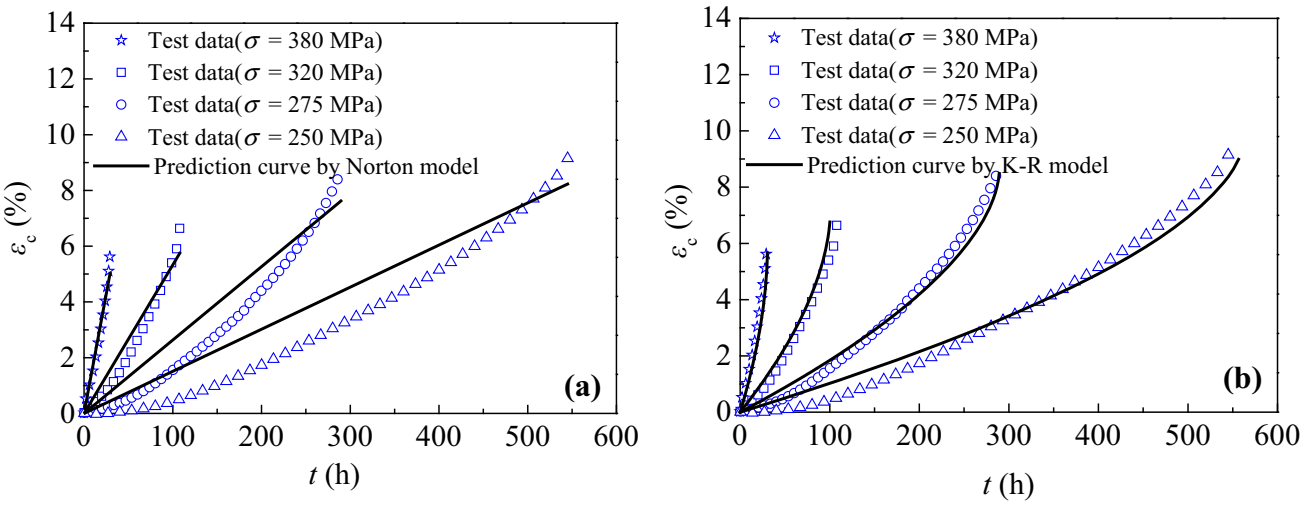

Fig. 4 Comparison of the uniaxial creep strain between the theoretical results and test data: the **a** Norton model and **b** K–R model

Table 5 Comparison of the RSS and *R*-squared for the two theoretical models

σ (MPa)	Norton model		K–R model	
	RSS	*R*-square	RSS	*R*-square
250	0.1560	0.868	0.0275	0.976
275	0.0632	0.885	0.0100	0.982
320	0.0216	0.842	0.0036	0.974
380	0.0017	0.972	0.0089	0.852

$t > 0.9t_r$, the ω value increases significantly. Thus, the operating time of the elevated temperature structure designed with the UNS N10003 alloy should not exceed 90% of the creep life t_r.

2.3.2 *Multi-axial stress state*

1. Creep strain analysis

The equivalent creep strain ε_{eq} is adopted to assess the creep behavior under the multi-axial stress state. Three components of the principal creep strain are assumed as ε_{11}, ε_{22}, and ε_{33}. The equation for ε_{eq} is as follows:

$$\varepsilon_{eq} = \sqrt{\frac{2}{9}\left[(\varepsilon_{11}-\varepsilon_{22})^2+(\varepsilon_{11}-\varepsilon_{33})^2+(\varepsilon_{22}-\varepsilon_{33})^2\right]} \quad (12)$$

In this study, a common multi-axial stress state in nuclear power engineering is analyzed and discussed. The three principal stress components are $\sigma_1 = 0$, $\sigma_2 = 2\sigma$, and $\sigma_3 = \sigma$. The curves of ε_{eq} versus t are plotted under the stress level of $\sigma = 100$ MPa, as shown in Fig. 6. The α values in the K–R model are 0, 0.5, and 1.0, respectively.

From Fig. 6, the Norton creep curves overlap with the K–R creep curves. The time of the intersection point is t_o. When $t = t_o$, the predicted values (ε_{eq}) of the two theoretical models are equal. When $t < t_o$, the ε_{eq} values of the Norton model are larger than those of the K–R model. When $t > t_o$, the ε_{eq} values of the Norton model are smaller than those of the K–R model. Based on these calculations, the results of the accumulated equivalent creep strain by the K–R model would be more conservative than those of the Norton model during long-term service. In addition, the value of α directly determines the variation of the K–R creep curves. When α varies from 0 to 1, the t_r and ε_r values predicted by the K–R model are decreased by 65%.

2. Creep damage analysis

The theoretical prediction values of the creep damage can be obtained using the K–R creep damage model under the

Table 6 Comparison between the K–R theoretical predicted values and test data

σ (MPa)	t_r (h)			ε_r		
	Theoretical values	Test data	Error (%)	Theoretical values	Test data	Error (%)
250	562.12	545.1	3.03	0.0969	0.0965	0.41
275	289.28	289.5	0.08	0.0858	0.0894	4.20
320	100.59	107.9	7.27	0.0707	0.0706	0.14
380	30.365	29.10	4.17	0.0567	0.0576	1.59

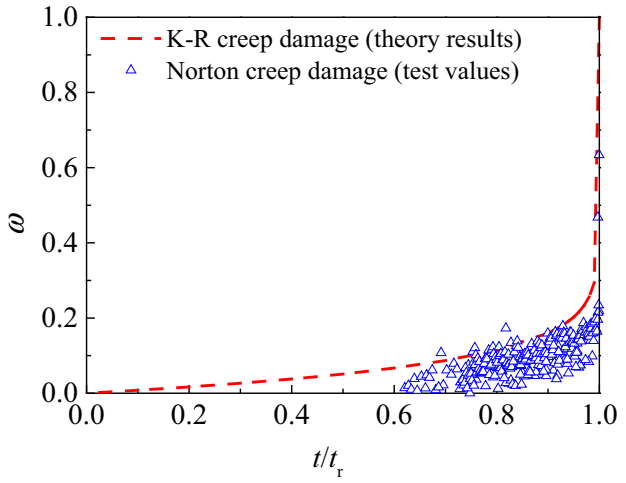

Fig. 5 (Color online) Comparison between the K–R creep damage and Norton creep damage under the uniaxial stress state

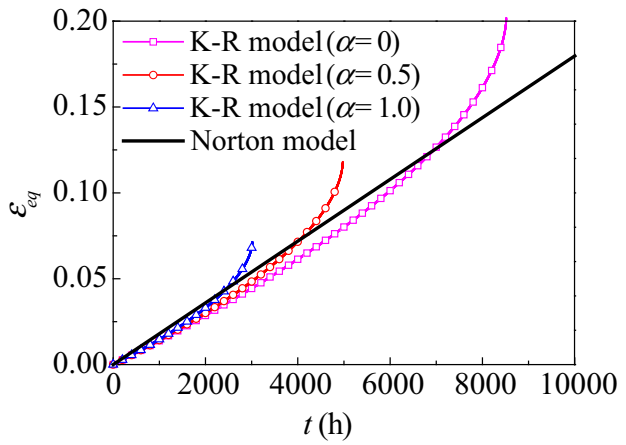

Fig. 6 Curves of the equivalent creep strain under the multi-axial stress state

multi-axial stress state. According to Eqs. (5) and (6), the K–R creep damage ω bears on the reference stress σ_r, which is related to the α value. The curves of ω versus time are plotted with $\alpha = 0$, 0.5, and 1.0 and are shown in Fig. 7. When $\alpha = 0$, $\sigma_r = \sigma_{eq} = 1.732\sigma$, and the ω value depends on σ_{eq}. When $\alpha = 0.5$, $\sigma_r = 0.5(\sigma_1 + \sigma_{eq}) = 1.867\sigma$, and the ω value depends on σ_{eq} and σ_1. When $\alpha = 1.0$, $\sigma_r = \sigma_1 = 2\sigma$, and the ω value depends on σ_1. Thus, the ω value depends on σ_{eq}, σ_1, and α under the multi-axial stress state. Furthermore, the accumulated creep damage gradually increases with the increase of α at the same time. When $t = 3000$ h, the ω value is equal to 0.0331 ($\alpha = 0$), 0.0691 ($\alpha = 0.5$), and 0.334 ($\alpha = 1.0$). The ω value with $\alpha = 1.0$ is approximately ten times than that with $\alpha = 0$. The α value affects the accumulated creep damage and time of the creep rupture.

The above analysis shows that the multi-axial creep damage is more complicated than the uniaxial creep

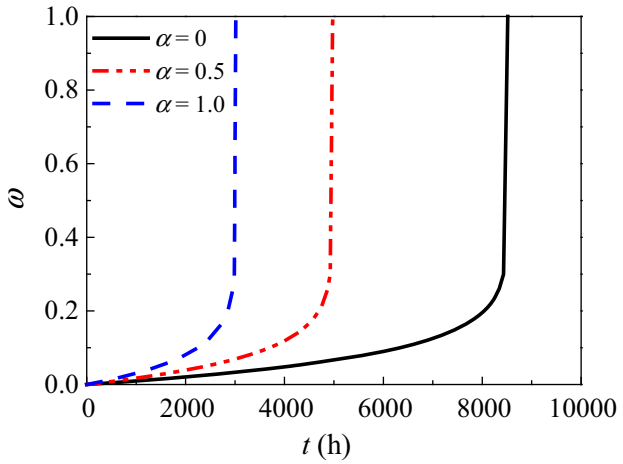

Fig. 7 Curves of the K–R creep damage ω versus α under the multi-axial stress state

damage. The material constant α influences the theoretical prediction values of the creep strain and creep damage. Thus, the α value of the UNS N10003 alloy should be measured by multi-axial creep tests.

3 Numerical calculations

3.1 Calculation method and the FEA model

In this study, only the elastic strain and creep strain are considered, while the influence of the initial plasticity on the inelastic strain [24, 25] is neglected. The ABAQUS code is a suite of powerful engineering simulation programs based on the finite element method, which can simulate the behavior of most typical engineering materials [26, 27]. The Norton model can be adopted for the creep analysis, which is embedded in the ABAQUS code. However, a user-defined material constitutive equation is required for the K–R creep damage model. In this study, a UMAT subroutine is compiled using FORTRAN language to develop the K–R creep damage model in ABAQUS software. The flow diagram of the UMAT subroutine is shown in Fig. 8.

The UMAT subroutine defines the Jacobin matrix of the material and updates the stress, strain, and state variables at the integration point. Two analysis steps are set. (1) In the elastic analysis, the relationship between the stress and strain is defined according to Hooke's law. (2) In the creep analysis, the creep damage equations (Eqs. (3) and (4)) are discretized with the central difference method to obtain the creep strain increment and damage increment. According to the initial strain method of the finite element increment theory, the nonlinear iteration is performed to update the

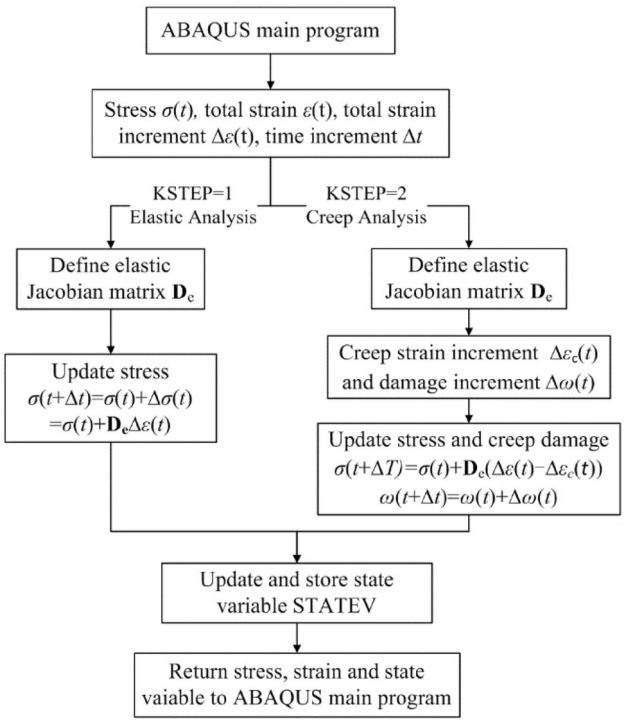

Fig. 8 Flow diagram of the UMAT subroutine

stress using the elastic stiffness matrix. The creep damage is updated as a state variable.

In order to verify the accuracy of the subroutine, two FEA models are established using ABAQUS software, as shown in Fig. 9. (1) A rectangular block (10 mm × 10 mm × 50 mm) is subjected to a uniform tensile stress. The model is meshed by 8-node hexahedron elements (C3D8). The number of nodes and elements is 3396 and 625, respectively. The tensile stress (250 MPa) is applied to one end, while the other end of the block is restrained (UZ = 0). This model can simulate the uniaxial stress state. (2) A thick-walled cylinder is subjected to internal pressure. The internal diameter, outer diameter, and length of the thick-walled cylinder are 1 m, 2 m, and 5 m, respectively. The model is also meshed by 8-node hexahedron elements (C3D8). The number of nodes and elements is 37,400 and 8400, respectively. The axial and circumferential displacements of both ends of the cylinder are constrained, and the radial displacement is free (UZ = UY = 0, UX = Free). An internal pressure (100 MPa) is applied to the inner wall of the cylinder. This model is used to simulate the multi-axial stress state.

In the simulation of the Norton model, the elastic material constants at 650 °C are set, for example, Young's modulus E = 178 GPa and Poisson's ratio υ = 0.31. In addition, the material constants C_1 and C_2 are inputted in the power law creep model. The creep analysis step is defined as Visco. In the simulation of the K–R model, the user materials are set, including E and υ, as well as the material constants of the K–R creep damage model (see Table 4). In addition, the user-defined output variables and the number of state variables (Depvar) are also inputted when editing the material behaviors.

3.2 Calculation results and discussion

3.2.1 *Uniaxial stress state*

The Norton and K–R models are adopted to analyze the creep behavior of a rectangular block model under the uniaxial stress state. A comparison between the creep strains of the FEA results and the theoretical solution is shown in Fig. 10. The FEA results of the Norton and K–R

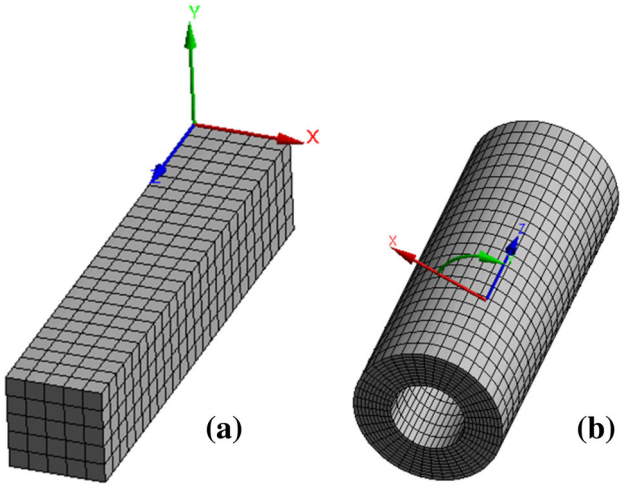

Fig. 9 Two FEA models for verifying the subroutine: **a** a rectangular block applied to the uniform tensile stress and **b** a thick-walled cylinder subjected to an internal pressure

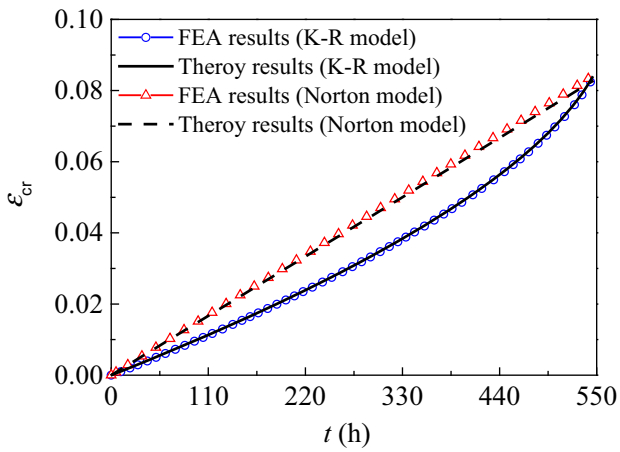

Fig. 10 (Color online) Comparison of the creep strain between the FEA results and theoretical solution under the uniaxial stress state

Table 7 Comparisons of the creep strain between the FEA results and theoretical solution

Creep model	Theoretical solution	FEA results	Error (%)
Norton model	0.0826	0.084	1.69
K–R model	0.0837	0.083	0.84

models are consistent with their theoretical prediction values.

The FEA results of the creep strain at $t = 540$ h are listed in Table 7. The results indicate that the maximum errors of the creep strain between the FEA results and theoretical solution are approximately 1.69% for the Norton model and 0.84% for the K–R model. Therefore, the K–R model is more accurate than the Norton model.

In order to determine the convergence of the numerical calculation by the UMAT subroutine, the creep strain increments $\Delta\varepsilon_c^{(n)}$ at iteration step n and the creep strain increments $\Delta\varepsilon_c^{(n+1)}$ at iteration step $n + 1$ are calculated. The ratio of $\left\|\Delta\varepsilon_c^{(n+1)} - \Delta\varepsilon_c^{(n)}\right\| / \left\|\Delta\varepsilon_c^{(n+1)}\right\|$ is obtained as the relative norm error [22]. During the iterations, the relative norm error gradually decreases and is stable. When the number of iteration reaches 2702, the minimum relative norm error is equal to 1.73×10^{-4} and lower than the admissible error (2×10^{-4} is defined). Therefore, the subroutine is adequate, and the calculation results are convergent.

3.2.2 *Multi-axial stress state*

The thick-walled cylinder subjected to an internal pressure leads to the multi-axial stress (radial stress σ_r, circumferential stress σ_θ, and axial stress sigma σ_z). The theoretical solutions of the stress components are available under the elastic state as well as the steady creep state for the thick-walled cylinder [21]. The FEA results by the Norton and K–R models are obtained and compared with the theoretical solution. The circumferential stress distribution curves of the thick-walled cylinder along wall thickness direction r are shown in Fig. 11. Figure 11a shows the elastic stress at $t = 0$. Figure 11b shows the creep stress at $t = 1000$ h. From the diagram, the redistribution of the circumferential stress is caused by creep relaxation. The FEA results of the creep stress are consistent with the theoretical solutions.

The FEA results of the creep stresses at the inner wall ($t = 1000$ h) are listed in Table 8 and compared with the

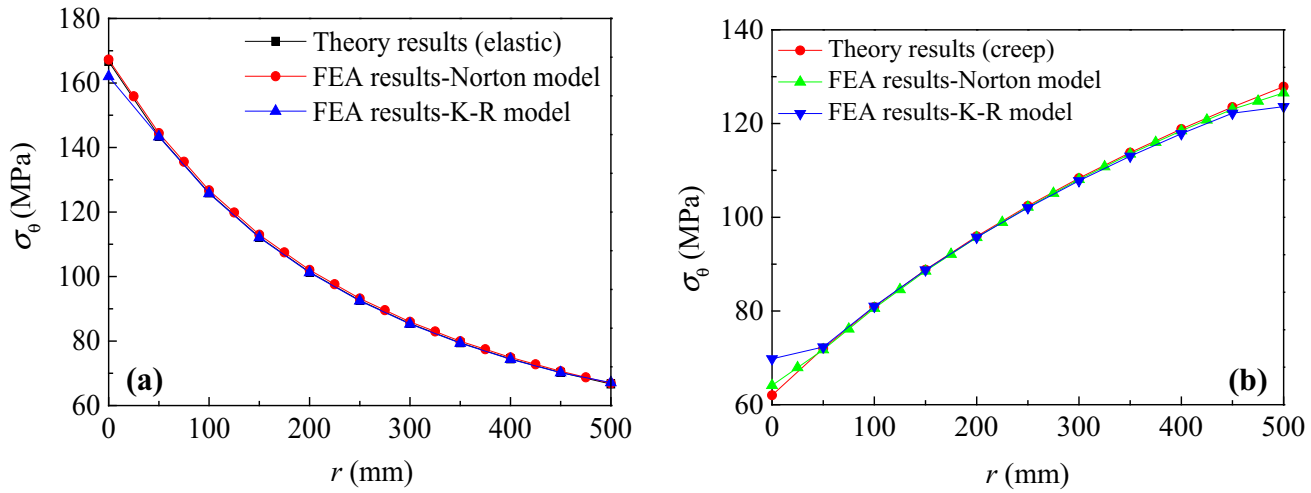

Fig. 11 (Color online) Circumferential stress distribution curves of the thick-walled cylinder along the r direction: **a** $t = 0$ and **b** $t = 1000$ h

Table 8 Comparisons of the creep stresses between the FEA results and theoretical solutions

σ (MPa)	Theoretical solutions	FEA results			
		Norton model	Error (%)	K–R model	Error (%)
σ_r	− 100.0	− 100.6	0.60	− 91.04	8.96
σ_θ	62.00	64.12	3.42	69.78	12.6
σ_z	− 18.99	− 16.13	15.1	− 14.36	24.4
σ_{eq}	140.3	142.7	1.69	139.9	0.69

theoretical solutions. The errors of the equivalent stress between the FEA results and the theoretical solutions are approximately 1.69% for the Norton model and 0.69% for the K–R model, which are within the permissible deviation range. Therefore, the multi-axial creep behavior can also be accurately simulated by the calculation method presented in this study. In addition, the FEA results of the K–R model are more accurate than those of the Norton model.

4 Conclusion

In this study, the material constants of the UNS N10003 alloy were obtained by fitting the creep test data. Then, the creep damage characterization was investigated using the Norton creep law and K–R creep damage model. The results indicated that the K–R model is more consistent with the test data, and hence more suitable for describing the creep behavior of the UNS N10003 alloy. In addition, the material constant α influenced the K–R creep damage; this aspect requires further investigation. Moreover, the numerical simulation method was developed by compiling the UMAT subroutine and subsequent verification through FEA. The FEA results were in agreement with the theoretical solutions. The theoretical models and numerical simulation method in this study are applicable to the creep damage calculation of the elevated temperature structures in the TMSR.

References

1. X.Z. Cai, Z.M. Dai, H.J. Xu, Thorium molten salt reactor nuclear energy system. Physics **45**, 578–590 (2016). https://doi.org/10.7693/wl20160904. **(in Chinese)**
2. J.J. Li, Y.L. Qian, J.L. Yin et al., Large eddy simulation of unsteady flow in gas–liquid separator applied in thorium molten salt reactor. Nucl. Sci. Tech. **29**, 62 (2018). https://doi.org/10.1007/s41365-018-0411-3
3. R.M. Ji, Y. Dai, G.F. Zhu et al., Evaluation of the fraction of delayed photoneutrons for TMSR-SF1. Nucl. Sci. Tech. **28**, 135 (2017). https://doi.org/10.10071/s41365-017-0285-9
4. ASME Boiler and Pressure Vessel Code, Section III, Division 1-Subsection NH, Class 1 Components in elevated temperature, Rules for Construction of Nuclear Facility Components (2015)
5. T. Asayama, S. Takaya, Y. Nagae et al., Creep-fatigue evaluation methodologies and related issues for Japan sodium cooled fast reactor (JSFR). Procedia Eng. **55**, 309–313 (2013). https://doi.org/10.1016/j.proeng.2013.03.259
6. G.H. Koo, J.J. Sienicki, C.P. Tzanos et al., Creep-fatigue design evaluations including daily load following operations for the advanced burner test reactor. Nucl. Eng. Des. **239**, 1750–1759 (2009). https://doi.org/10.1016/j.nucengdes.2009.05.010
7. G.H. Koo, J.J. Sienicki, A. Moisseytsev, Preliminary structural evaluations of the STAR-LM reactor vessel and the support design. Nucl. Eng. Des. **237**, 802–813 (2007). https://doi.org/10.1016/j.nucengdes.2006.11.004
8. H.Y. Lee, J.B. Kim, H.Y. Park, Creep-fatigue damage evaluation of sodium to air heat exchanger in sodium test loop facility. Nucl. Eng. Des. **250**, 308–316 (2012). https://doi.org/10.1016/j.nucengdes.2012.05.034
9. F. Yousefpour, S.M. Hoseyni, S.M. Hoseyni et al., Creep rupture assessment for level-2 PSA of a 2-loop PWR: accounting for phenomenological uncertainties. Nucl. Sci. Tech. **28**, 107 (2017). https://doi.org/10.1007/s41365-017-0269-9
10. H.J. Yu, *Structural Mechanics of Fast Reactor* (Atomic Energy Press, Beijing, 2016), pp. 61–69. **(in Chinese)**
11. F.H. Norton, *The Creep of Steel at High Temperatures* (McGraw-Hill, London, 1929)
12. X.P. Mao, Q. Guo, S.Y. Zhang et al., Study on creep damage behaviors of Ni-based alloy C276. Nucl. Power Eng. **34**, 86–89 (2013). https://doi.org/10.3969/j.issn.0258-0926.2013.02.020. **(in Chinese)**
13. A.A. Becker, T.H. Hyde, W. Sun et al., Benchmarks for finite element analysis of creep continuum damage mechanics. Comput. Mater. Sci. **25**, 34–41 (2002). https://doi.org/10.1016/j.commatsci.2004.09.046
14. T.H. Hyde, A.A. Becker, A. Sun et al., Finite-element creep damage analyses of P91 pipes. Int. J. Pres. Ves. Pip. **83**, 853–863 (2006). https://doi.org/10.1016/j.ijpvp.2006.08.013
15. T. Hyde, L. Xia, Prediction of creep failure in aeroengine material under multi-axial stress states. Int. J. Mech. Sci. **38**, 385–403 (1996). https://doi.org/10.1016/0020-7403(95)00063-1
16. Z.H. Du, D.H. Liu, Y.H. Liu, Numerical limit load analysis of 3D pressure vessel with volume defect considering creep damage behavior. Math. Probl. Eng. **6**, 1–13 (2015). https://doi.org/10.1155/2015/204730
17. X.C. Niu, J.M. Gong, Y. Jiang et al., Creep damage prediction of the steam pipelines with high temperature and high pressure. Int. J. Pres. Ves. Pip. **86**, 593–598 (2009). https://doi.org/10.1016/j.ijpvp.2009.04.014
18. J.T. Bao, Dissertation, Nanjing University of Technology, 2006
19. J. Lemaitre, How to use damage mechanics. Nucl. Eng. Des. **80**, 233–245 (1984). https://doi.org/10.1016/0029-5493(84)90169-9
20. H.T. Yao, F.Z. Xuan, Z.D. Wang et al., A review of creep analysis and design under multiaxial stress states. Nucl. Eng. Des. **237**, 1969–1986 (2007). https://doi.org/10.1016/j.nucengdes.2007.02.003
21. H.T. Yao, Dissertation, East China University of Science and Technology, 2008 **(in Chinese)**
22. ASME Boiler and Pressure Vessel Code, Section II, Materials, Part B, Nonferrous Material Specifications, Rules for Construction of Nuclear Facility Components (2017)
23. F.A. Leckie, D.R. Hayhurst, Constitutive equations for creep rupture. Acta Metall. **25**, 1059–1070 (1977). https://doi.org/10.1016/0001-6160(77)90135-3
24. S.D. Tu, *Principle of High Temperature Structural Integrity* (Science Press, Beijing, 2003), pp. 256–289. **(in Chinese)**
25. M.C. Wang, *Finite Element Method* (Tsinghua University Press, Beijing, 2003), pp. 185–191. **(in Chinese)**
26. Sh Sheykhi, S. Talebi, M. Soroush et al., Thermal-hydraulic and stress analysis of AP1000 reactor containment during LOCA in dry cooling mode. Nucl. Sci. Tech. **28**, 73 (2017). https://doi.org/10.1007/s41365-017-0233-8
27. Y. Zhong, X. Yang, D. Dong et al., Numerical study of the dynamic characteristics of a single-layer graphite core in a thorium molten salt reactor. Nucl. Sci. Tech. **29**, 141 (2019). https://doi.org/10.1007/s41365-018-0488-8